BIOCHEMISTRY
including biophysical chemistry & molecular biology

Article

pubs.acs.org/biochemistry

The Crystal Structure of Necrosis- and Ethylene-Inducing Protein 2 from the Causal Agent of Cacao's Witches' Broom Disease Reveals Key Elements for Its Activity

Gustavo Zaparoli,[†,‡] Mario Ramos de Oliveira Barsottini,[†,‡] Juliana Ferreira de Oliveira,[‡] Fabio Dyszy,[§] Paulo José Pereira Lima Teixeira,[†] Joan Grande Barau,[†] Odalys Garcia,[†] Antonio José Costa-Filho,[§] Andre Luis Berteli Ambrosio,[‡] Gonçalo Amarante Guimarães Pereira,[†,‡] and Sandra Martha Gomes Dias*[,‡]

[†]Departamento de Genética e Evolução, IB/UNICAMP, C.P. 6109, 13083-970 Campinas, SP, Brazil

[‡]Laboratório Nacional de Biociências-LNBio, Associação Brasileira de Tecnologia de Luz Síncrotron, 13083-970 Campinas, SP, Brazil

[§]Grupo de Biofísica Molecular Sérgio Mascarenhas, Instituto de Física de São Carlos, Universidade de São Paulo, C.P. 369, 13560-970 São Carlos, SP, Brazil

Supporting Information

ABSTRACT: The necrosis- and ethylene-inducing peptide 1 (NEP1)-like proteins (NLPs) are proteins secreted from bacteria, fungi and oomycetes, triggering immune responses and cell death in dicotyledonous plants. Genomic-scale studies of *Moniliophthora perniciosa*, the fungus that causes the Witches' Broom disease in cacao, which is a serious economic concern for South and Central American crops, have identified five members of this family (termed MpNEP1−5). Here, we show by RNA-seq that MpNEP2 is virtually the only NLP expressed during the fungus infection. The quantitative real-time polymerase chain reaction results revealed that MpNEP2 has an expression pattern that positively correlates with the necrotic symptoms, with MpNEP2 reaching its highest level of expression at the advanced necrotic stage. To improve our understanding of MpNEP2's molecular mechanism of action, we determined the crystallographic structure of MpNEP2 at 1.8 Å resolution, unveiling some key structural features. The implications of a cation coordination found in the crystal structure were explored, and we show that MpNEP2, in contrast to another previously described member of the NLP family, NLP_{Pya} from *Pythium aphanidermatum*, does not depend on an ion to accomplish its necrosis- and electrolyte leakage-promoting activities. Results of site-directed mutagenesis experiments confirmed the importance of a negatively charged cavity and an unforeseen hydrophobic β-hairpin loop for MpNEP2 activity, thus offering a platform for compound design with implications for disease control. Electron paramagnetic resonance and fluorescence assays with MpNEP2 performed in the presence of lipid vesicles of different compositions showed no sign of interaction between the protein and the lipids, implying that MpNEP2 likely requires other anchoring elements from the membrane to promote cytolysis or send death signals.

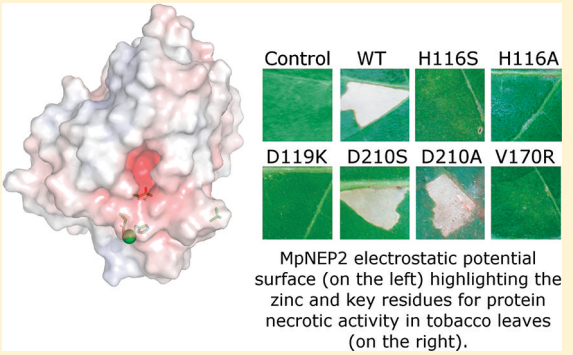

MpNEP2 electrostatic potential surface (on the left) highlighting the zinc and key residues for protein necrotic activity in tobacco leaves (on the right).

Witches' Broom disease of cacao (*Theobroma cacao*), the raw material for chocolate production, is well-regarded as one of the most important phytopathological problems to afflict the southern hemisphere in recent decades, with devastating consequences to the agro-economy of the affected countries.[1] In Brazil, this disease started as an endemic disease within the Amazon region, but after an outbreak in 1989, it was introduced into the largest area of cacao production, the state of Bahia.[2] A severe decrease in the production of cacao then followed, and in less than a decade, Brazil shifted from being the second largest cacao exporter to being a cacao importer. World chocolate production could fall dramatically if this disease, which has devastated South and Central American crops over the past 20 years, were to spread to some of the world's other cacao-producing regions.[3]

Moniliophthora perniciosa, the causal agent of Witches' Broom disease, is a basidiomycete with a hemibiotrophic life cycle.[4,5] Initially, mononucleated basidiospores, dispersed by the wind and rain at night, germinate on rapidly growing tissues, such as meristems and young pods, initiating the biotrophic phase of the disease. When emerging branches are infected, the disease is characterized by an impressive growth of new shoots (green broom), which probably acts as a nutritional sink.[5,6] Eight to twelve weeks after the initial infection, the tissues begin to senesce and are colonized inter- and

Received: August 9, 2011
Revised: October 13, 2011
Published: October 14, 2011

intracellularly by the saprotrophic mycelia of *M. perniciosa*. The transition from biotrophic to necrotrophic involves changes not only in the plant but also in the biology of the vegetative mycelia.[7−9] The senescing brooms turn brown, forming the typical necrotic dry broom structures of this disease, which remain attached to the plant. After a dry period of 3−9 months, the brooms produce basidiocarps that release spores into the air and reinitiate the disease cycle.[5] Infected plants produce fewer and lower-quality fruits, compromising the amount of cocoa beans produced.[1]

In recent years, efforts have been made toward understanding the infection process at a molecular level and its correlation with the fungus life cycle.[3] Genomic-scale studies have identified key components resulting from the *M. perniciosa*−cacao interaction. Among them, five DNA sequences encoding putative copies of proteins in the fungus that are similar to the necrosis- and ethylene-inducing peptide 1 (NEP1)-like proteins (NLPs) were identified and have been termed MpNEP1−5.[10,11] NLPs are proposed to perform dual functions in the plant−pathogen interactions, acting both as triggers of immune responses and as toxin-like virulence factors known to promote leaf necrosis.[12] The family contains members from the genomes of more than 50 organisms, including fungi, oomycetes, and bacteria, with either saprotrophic or hemibiotrophic lifestyles.[13] Members of the NLP family share a high degree of sequence similarity, containing a secretory signal sequence, a conserved seven-amino acid motif (GHRHDWE), and two or four conserved cysteine residues. The proteins from this family induce a hypersensitive-like death response in a variety of dicotyledonous plants but not in any known monocotyledonous plants.[14]

Here, we provide evidence that MpNEP2 is strongly expressed during the necrotic stage of the fungus infection. To understand the molecular mechanism of action of MpNEP2, we determined its crystallographic structure at 1.8 Å resolution. The crystal structure data combined with the results of site-directed mutagenesis experiments and functional assays highlighted the importance of the conserved seven-amino acid motif (GHRHDWE) and an unforeseen hydrophobic loop in the necrotic process, offering the basis for the design of compounds with the potential to inhibit the protein. Moreover, to test MpNEP2's potential role as a lipid-binding protein, we performed electron paramagnetic resonance (EPR) studies of four different headgroup and acyl chain spin probe phospholipid vesicles added to MpNEP2, as well as tryptophan fluorescence measurements of MpNEP2 added to equivalent nonlabeled vesicles. The results indicated no change in the EPR spectra of the tested lipids and no significant shift in the tryptophan intensity or wavelength emission peak when the protein was added to the vesicles described above, raising the possibility that, if the protein interacts with the cell membrane to perform its necrotic activity, it likely requires some other anchoring element.

EXPERIMENTAL PROCEDURES

RNA-seq and Quantitative Polymerase Chain Reaction (PCR). *T. cacao* var. Comum was cultivated in a greenhouse under controlled temperature and humidity conditions (from 22 to 28 °C and >50%, respectively). Two-month-old seedlings were then infected with *M. perniciosa* spores as described previously.[15] RNA-seq libraries that were produced as part of the WBD Transcriptome Atlas were inspected for the expression of NLP genes during the *in planta* development of *M. perniciosa*, from the green broom to the dry broom stage (where the plant is virtually consumed by the fungus). The RNA-seq methodology will be described elsewhere (P. L. Teixeira, manuscript in preparation). For the qPCR assays, plant material was collected at five different stages of the disease progression, as follows: no symptoms (10 DAI), first symptoms (swelling, 20 DAI), mature green broom (green broom, 30 DAI), first necrosis symptoms (initial necrosis, 60 DAI), and advanced necrosis (100 DAI). RNA extraction was performed as described by Azevedo and colleagues with minor modifications;[16] the cDNA was synthesized using a SuperScript VILO cDNA Synthesis Kit (Invitrogen), and real-time PCR was conducted according to the Delta-Delta-CT method[17] using primers F-AAGGCAAGACTGCTCTGGTCTA and R-CTTCCTTTCCATCGTCCTTCTCGT and the tubulin gene for endogenous housekeeping.

Heterologous MpNEP2 Production. We constructed a truncated form of MpNEP2 (GenBank accession number EF114673.1) that had its secretion signaling peptide deleted (residues Met1−Ala17). This construct (hereafter termed MpNEP2) was cloned into a modified version of the pETSUMO plasmid (Invitrogen), which contains a histidine tag at its N-terminus, and was used to transform *Escherichia coli* Origami 2 cells (Merck). The cells were lysed, and the clarified soluble fraction was purified by a two-step procedure starting with immobilized metal ion affinity chromatography (IMAC) using a Co^{2+}-charged TALON resin (BD Biosciences) pre-equilibrated with 30 mM Tris-HCl (pH 8.0), 150 mM NaCl, 5 mM imidazole, 0.3 mM TCEP [tris(2-carboxyethyl)phosphine hydrochloride], and 1 mM PMSF (phenylmethanesulfonyl fluoride). The resin was washed extensively with this solution and then incubated overnight at room temperature with an appropriate amount of protease ULP-1 for His-SUMO tag removal. The cleaved protein was eluted from the resin and loaded onto a HiLoad Superdex 75 16/60 gel filtration column (GE Healthcare) pre-equilibrated in 30 mM Tris-HCl (pH 8.0) and 50 mM NaCl. The eluted protein was concentrated to 19 mg/mL as judged by its UV_{280} absorption and calculated coefficient extinction[18] and used for crystallization screens and functional assays. Mutants were obtained with the QuikChange Site-Directed Mutagenesis Kit (Stratagene) by following the manufacturer's instructions and purified according to the protocol developed for the wild-type protein.

X-ray Crystallography. The crystallization experiments were performed at 18 °C using the conventional sitting drop vapor diffusion technique. The drops were made by mixing equal parts of protein and well solution, the latter containing 100 mM sodium acetate (pH 5.0), 20% PEG 6000, and 200 mM $ZnCl_2$. Before data collection at cryogenic temperatures, the harvested crystals were cryoprotected with 5% ethylene glycol added to the mother liquor. A substantially complete X-ray diffraction data set for MpNEP2 was obtained with beamline D03B-MX1 at the Brazilian National Synchrotron Laboratory at a wavelength of 1.608 Å.

Phasing and Refinement. The X-ray diffraction data were processed using Mosflm[19] and merged and scaled with SCALA.[20] The first set of phases was obtained by the molecular replacement technique as implemented in Phaser,[21] using the *Pythium aphanidermatum* NEP_{Pya} monomer (deposited as Protein Data Bank entry 3gnz[22]) as the search model. Following molecular replacement, a density modification was performed using Parrot, which is part of the CCP4 suite,[23,24] and the improved map was then subjected to an automated

interpretation with the ARPwARP routine.[25] The positional and *B* factor refinement cycles were performed with Refmac.[26] The manual building of the extra portions and real space refinement, including a Fourier electron density map inspection, were performed with Coot.[27] The solvent water molecules, which were treated as oxygen atoms, were added using the appropriate Coot routine. FFT, part of the CCP4 suite,[24,28] was used to calculate the Fourier anomalous electron density map. The overall stereochemical quality of the final model and the agreement between the model and the experimental data were assessed with Molprobit[29] and the appropriate Coot routines.

Circular Dichroism. MpNEP2 (6 μM, wild type and mutants) was dialyzed against 4 mM sodium phosphate buffer (pH 7.2), and when required, EDTA (62.5 μM) or both EDTA (62.5 μM) and $CaCl_2$ with $ZnCl_2$ (120 μM) were added. The samples were analyzed by far-UV CD spectroscopy (190−260 nm) with a resolution of 1 nm using a JASCO J810 spectropolarimeter. Each data point was generated by averaging 10 accumulations. The secondary structure was estimated on a DICHROWEB interface[30] using the CDSSTR method[30] and Reference Protein Set 4. The mean residue molar ellipticity at 218 nm (MRE $[\theta]_{218}$) was also collected at temperatures ranging from 20 to 60 °C at intervals of 1 °C. The apparent melting temperature (T_{Mapp}), which is the temperature at which the molar ellipticity is between the folded and unfolded states, was used to estimate the stability of the wild-type and mutant protein. The data were analyzed using Origin (OriginLab Corp.) for a sigmoidal fit and an inflection point calculation (T_{Mapp}).

Dynamic Light Scattering. A DynaPro MSTC014 (Protein Solutions Inc., Lakewood, NJ) dynamic light scattering instrument was used to monitor the oligomeric state of MpNEP2 at concentrations between 220 and 260 μM in 4 mM sodium phosphate buffer (pH 7.2) in the absence or presence of either EDTA, $CaCl_2$, or $ZnCl_2$ (1 mM). The assays were performed at 20 °C with an acquisition time of 5−8 s using a 70 μL cuvette and 50−100% laser power. Three hundred acquisitions were obtained in a single measurement, and a PBS solution was used for the calculation of the hydrodynamic radii (R_H) by DYNAMICS version 6.1 (Protein Solutions Inc.). The theoretical R_H value for the monomeric protein was calculated by HYDROPRO[31] using the crystallographic model.

Infiltration of Purified MpNEP2 into Tobacco Leaves. The control solutions, wild-type MpNEP2 and mutants diluted to 500 nM in 10 mM sodium phosphate buffer (pH 7.2), were injected into leaves of *Nicotiana tabacum* var. Petite Havana (4−6 weeks old) as described previously.[11] The infiltration of MpNEP2 in BAPTA-containing buffer (10 mM), a specific calcium ion chelator, was preceded by the infiltration of the same leaves with 10 mM sodium phosphate buffer (pH 7.2) and 10 mM BAPTA. The formation of lesions was documented 5 days after the infiltration of MpNEP2.

Electrolyte Leakage Assay. The electrolyte leakage assay was conducted according to the method of Ottmann and colleagues[22] with modifications. The control solutions, containing purified wild-type or mutant MpNEP2, were injected into tobacco leaves as described above. The infiltrated area was immediately removed, cut into pieces of approximately 0.25 cm^2, and washed with distilled water. After 30 min, the pieces were transferred to fresh Milli-Q water (20 per replica in triplicate), and the intracellular content leakage was measured with a conductivity meter (WTW LF 330, Wissenschaftlich-Technische Werkstätten GmbH) at different time points.

Electron Paramagnetic Resonance (EPR) Spectroscopy. The phospholipids 1,2-dioleoyl-*sn*-glycero-3-phosphocholine (DOPC), 1-palmitoyl-2-oleoyl-*sn*-glycero-3-phospho(1′-*rac*-glycerol) (POPG), 1-palmitoyl-2-oleoyl-*sn*-glycero-3-phospho-L-serine (POPS), 1,2-dioleoyl-*sn*-glycero-3-phosphoethanolamine (DOPE), L-α-phosphatidylcholine from egg yolk (egg PC), and the EPR probes 1-palmitoyl-2-stearoyl(16-doxyl)-*sn*-glycero-3-phosphocholine (16-PC) and 1,2-dipalmitoyl-*sn*-glycero-3-phospho(tempo)choline (DPPTC) were purchased from Avanti Polar Lipids (Alabaster, AL). These lipids were chosen because of their high natural abundance in cell membranes.[32,33] The multilamellar liposomes were prepared by drying appropriate amounts of chloroform stock solutions of DOPC, DOPC and POPG (2:1 molar ratio), DOPC and POPS (2:1 molar ratio) and egg PC and DOPE (2:1 molar ratio) under a stream of N_2. The EPR spin probes were mixed with the DOPC, DOPC/POPG, DOPC/POPS, and egg PC/DOPE chloroformic solutions to give a final concentration of 0.5 mol %. The samples remained under vacuum for 2 h for the removal of the residual solvent, and the dried lipid film was resuspended at a total lipid concentration of 23.8 mM in 4 mM sodium phosphate (pH 7.2). The large unilamellar vesicles (LUVs) were prepared by extruding the multilamellar liposomes with a two-syringe extruder (Avanti Polar Lipids) equipped with two stacked polycarbonate filters with pores with an average diameter of 100 nm (Nucleopore). The continuous wave (CW) EPR spectroscopy experiments were conducted at room temperature (22 ± 1 °C) on a Varian E109 spectrometer operating at X-band. A measured amount of the buffered MpNEP2 solution was added to the suspension of LUVs and incubated for 10 min at room temperature. A final volume of 40 μL of the samples containing MpNEP2/DOPC/spin-label (DPPTC or 16-PC), MpNEP2/DOPC/POPG/spin-label (DPPTC or 16-PC), MpNEP2/DOPC/POPS/spin-label (DPPTC or 16-PC), or MpNEP2/egg PC/DOPE/spin-label (DPPTC or 16-PC) mixtures was drawn into a capillary tube, which was placed in the EPR resonant cavity. Control samples consisted of an LUV suspension without MpNEP2. The final enzyme concentration was 119 μM, and the protein:lipid molar ratio was 1:100. The acquisition conditions were as follows: modulation amplitude, 1.0 G; modulation frequency, 100 kHz; microwave power, 10 mW; field range, 160 G.

Intrinsic Fluorescence Measurements. The fluorescence measurements were recorded on a plate reader spectrofluorimeter (EnVision, Perkin-Elmer) using a 96-well all-black-walled Eppendorf plate and the default configurations of the equipment at 25.5 °C. The intrinsic fluorescence emission spectra of 2 μM MpNEP2 in 4 mM sodium phosphate (pH 7.2) were recorded from 310 to 500 nm after excitation at 295 nm to obtain the fluorescence spectra derived only from the tryptophan residues. The background intensities were always subtracted. Changes in the intrinsic fluorescence of MpNEP2 were also measured upon the addition of 200 μM of the following extruded LUVs: DOPC, DOPC/POPG (2:1 molar ratio), DOPC/POPS (2:1 molar ratio), and DOPC/DOPE (2:1 molar ratio).

RESULTS

The Level of MpNEP2 Expression Reaches Its Highest Point at the Necrotic Stage of the Disease. *M. perniciosa* has five copies of NLP genes in its genome.[10,11] An inspection

of RNA-seq libraries that were produced as part of the WBD Transcriptome Atlas (P. L. Teixeira, manuscript in preparation) revealed that only MpNEP2 was significantly expressed during an *in planta* experiment, in which cacao plants were infected with *M. perniciosa*, and samples were collected at different stages of the disease (Figure 1A). Moreover, results of a quantitative real-time PCR assay confirmed that the level of MpNEP2 expression increased along with the extent of the necrosis symptoms, reaching its peak at the advanced necrotic stage when the dry broom symptoms were noticeable (Figure 1B, bottom panel). These results are consistent with the previously described activity of NLP proteins[14] and suggest that MpNEP2 may be the major isoform involved in the necrosis of cacao during the Witches' Broom disease. On the basis of these findings, this protein was selected for additional structural analyses.

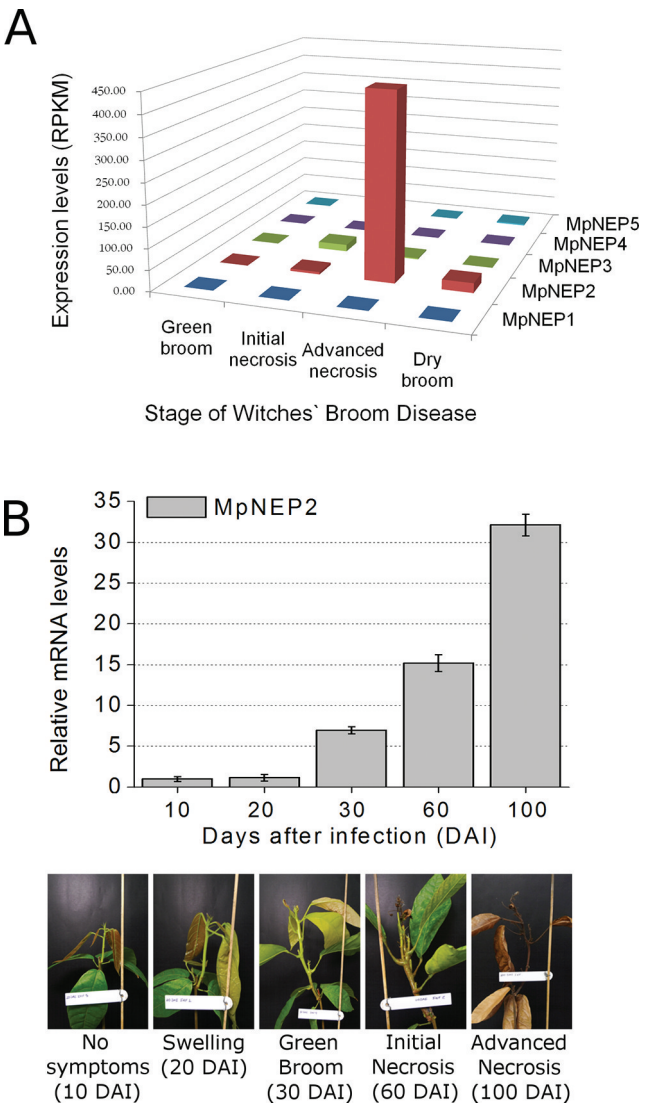

Figure 1. RNA-seq and real-time PCR analysis of MpNEP2 expression during Witches' Broom disease. (A) The RNA samples extracted from the green broom to the dry broom stages of WBD were sequenced and revealed that MpNEP2 is the major NLP found during the development of the disease (NCBI reference numbers EF109894 for MpNEP1, EF114673.1 for MpNEP2, EF164925 for MpNEP3, JN545833 for MpNEP4, and JN545834 for MpNEP5). (B) Real-time PCR confirmed a positive correlation between increasing levels of MpNEP2 and the appearance of necrotic symptoms. The disease stages, illustrated in the bottom panel, were classified as follows: no symptoms (10 DAI), beginning of swelling branches (20 DAI), mature green broom (30 DAI), beginning of necrosis in leaves (60 DAI), and advanced necrosis in branches (100 DAI). The dry broom stage is not shown. RPKM means reads per kilobase of exon model per 1 million mapped reads.

MpNEP2 Crystal Structure. Because we were interested in obtaining an improved understanding on the structural determinants of MpNEP2's mode of action, we determined the crystal structure of MpNEP2 at 1.8 Å resolution. The statistics of the final model are listed in Table 1. According to the Conserved Domain Database,[34] the structure belongs to the NPP1-like necrosis-inducing protein family. The overall architecture of the monomer in the asymmetric unit reveals a single-domain molecule with a fold consisting of a central β-sandwich, with three parallel strands in the first sheet and a five-stranded antiparallel sheet. Three α-helices ($\alpha1-\alpha3$) surround the second sheet, giving rise to a flat surface. Two large loops (loops 1 and 2) compose the other half of the polypeptide. The formation of an intramolecular disulfide bridge between two conserved cysteine residues within loop 2 (Figure S1 of the Supporting Information), reported to be essential for NLP

Table 1. Parameters and Statistics of Diffraction Data and Refinement[a]

Data Collection	
beamline	D03B-MX1 at LNLS
wavelength (Å)	1.608
space group	C121
unit cell dimensions	a = 89.48 Å, b = 44.21 Å, c = 60.17 Å, β = 110.04°
no. of monomers per asymmetric unit	1
resolution range (Å)	14.52−1.8 (1.9−1.8)
no. of unique reflections	19327 (2522)
average multiplicity	5.1 (3.7)
completeness (%)	93.9 (84.2)
R_{sym} (%)	0.049 (0.170)
$\langle(I)/\sigma(I)\rangle$	24.7 (7.9)
solvent content (%)	50.69
Refinement Statistics and Model Quality	
resolution range (Å)	20−1.8
total no. of reflections used	18298
no. of reflections for R_{free} calculation	1006 (5.2%)
R_f (%)/R_{free} (%)	14.22/19.57
no. of non-H atoms	1945
no. of residues	212
no. of waters	358
average B factor/rmsd (Å)	
main chain	12.6/0.8
side chain	13.56/1.78
solvent	26.16
rmsd from ideal bond length (Å)	0.021
rmsd from ideal angle (deg)	1.924
Ramachandran plot	
most favored region (%)	96.65
additional allowed region (%)	1.91
generously allowed region (%)	1.44

[a]The numbers in parentheses refer to the highest-resolution shell.

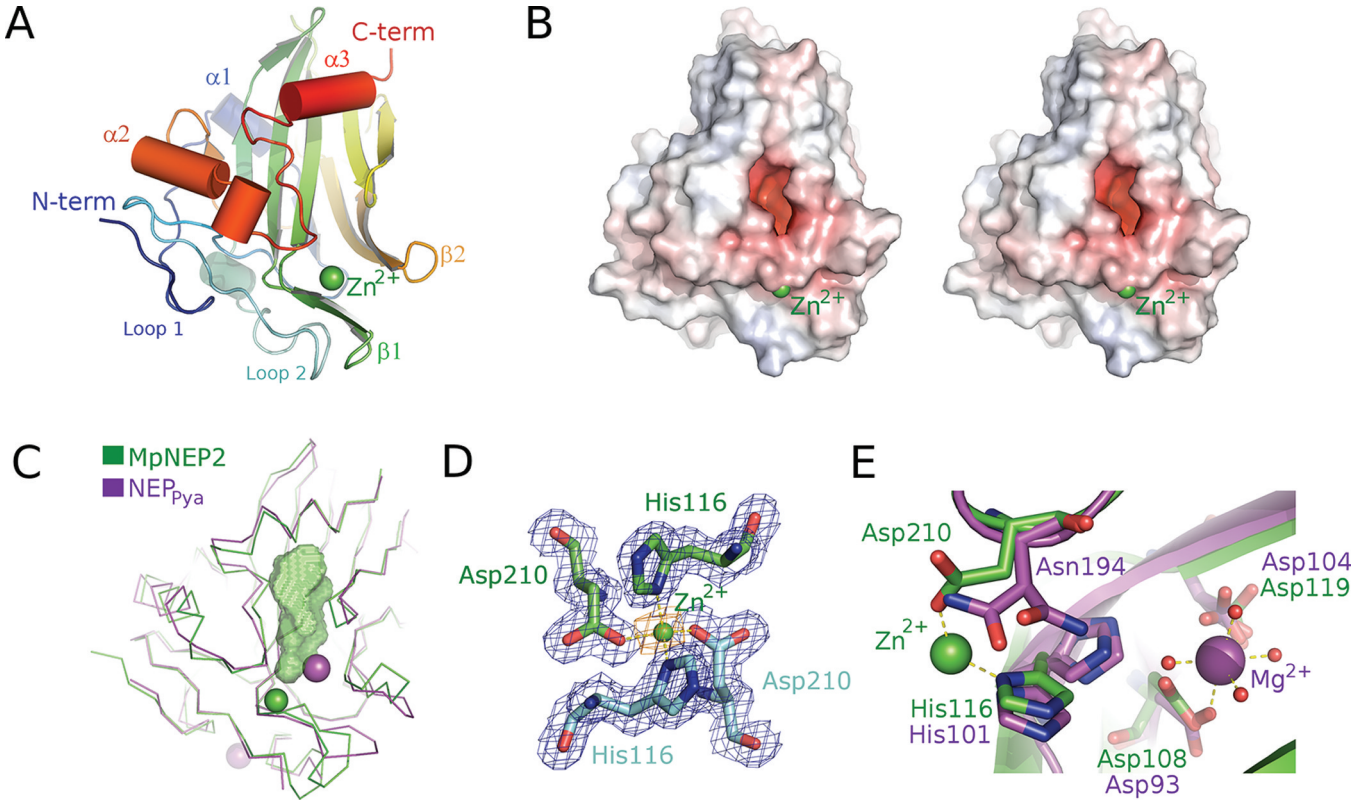

Figure 2. Crystal structure of MpNEP2. (A) Cartoon representation of MpNEP2 with a rainbow coloring scheme from blue (N-terminus) to red (C-terminus) and a text indication of its structural features, including the presence of a zinc ion (green sphere). (B) Stereoview of the electrostatic potential surface mapping calculated by APBS.[32] The color scale that varies from blue to red represents a variation from positive to negative potential, respectively ($\pm 12 k_b T_C e^{-1}$). This panel shows the presence of a very negatively charged cavity and its relative position to the zinc ion. (C) Ribbon representation of the structural superposition of MpNEP2 and NLP_{Pya} (green and purple ribbons, respectively), indicating both the high level of structural identity and distinct positions of the cations in the two models (zinc represented as a green sphere and magnesium represented as a purple sphere). The anionic cavity of MpNEP2 is represented as a green surface. (D) Fourier electron density map, $2F_o - F_c$ (blue mesh), for the residues coordinating to the zinc ion (green sphere), from both symmetry mates, represented as green and cyan sticks. The Fourier anomalous map (orange mesh), at 3σ level, contours the ion. (E) Specifics of the cation coordination in the crystallographic models. Whereas magnesium (purple sphere) is found inside the anionic cavity and is coordinated by Asp93 and Asp104, in the crystal structure of NLP_{Pya}[22] (represented as purple sticks), zinc (green sphere) is coordinated by His116 and Asp210 at the external surface of MpNEP2 (represented as green sticks).

activity,[14] appears to be crucial in stabilizing this loop closer to the β-sheet core of the protein. We can also identify the presence of two small 3_{10}-helices and two adjacent β-hairpins (β1 and β2). The structural features are illustrated in Figure 2A.

Electrostatic surface mapping, using APBS,[35] shows the presence of a strong negatively charged cavity (Figure 2B,C) formed among the five-stranded β-sheet, the loop between helices α2 and α3, and hairpin β1. A strand composed of the conserved sequence "GHRHDWE" defines the bottom of the cavity, which has a volume of 350 Å^3 (Figure 2C), as determined by the 3V server.[36] The negative potential is a contribution of the acidic side chains of Asp108, Asp119, and Glu121 and the main chain carboxyl groups of His118 and Trp120.

We observe a very strong peak, surrounding this cavity, in the Fourier $2F_o - F_c$ electron density map (>10σ in height), which, with respect to its contribution to the dispersive component of the scattering factor, was interpreted as a zinc ion (Figure S1 of the Supporting Information). This ion sits in a 2-fold center of symmetry in the crystal and is coordinated by the side chains of His116 and Asp210 from both the asymmetric unit monomer and its symmetry-related mate (Figure 2D). According to the PISA server,[37] there is an increase in free energy of −24.3 kcal/mol upon ion coordination; however, the resulting protein−protein interface is energetically less favored (0.9 kcal/mol, with a buried interface area of 580 Å^2). A second ion was also modeled on the opposite side of the protein surface, and using the same criteria for the determination of the zinc ion, it was interpreted to be sodium (Figure S1 of the Supporting Information). This cation is coordinated by the side chains of Asp157 and His53, the latter belonging to a symmetry-related monomer. Both zinc and sodium ions are present in the protein solution used for the crystallization at concentrations of 200 mM ($ZnCl_2$) and 50 mM (NaCl), respectively.

MpNEP2 Activity Is Not Ion-Dependent. Ottmann and co-workers[22] showed that the coordination of a divalent cation was crucial to NLP_{Pya} cytolytic activity. In this case, a magnesium ion was found inside the boundaries of a negatively charged cavity in the NLP_{Pya} structure, being coordinated directly by Asp93 and Asp104 (numbering according to NLP_{Pya}'s reference sequence) and four water molecules (Figure 2E). The overall MpNEP2 structure has a fold that is very similar to that of NLP_{Pya} (core rmsd of 1.08 Å), according to Lsqkab,[38] with the major difference between the two structures being the location of their divalent cation, as shown in Figure 2C. Nevertheless, Ottmann and co-workers presented evidence that Mg^{2+} was likely not a physiological ligand, and Ca^{2+} might actually be relevant for protein activity because BAPTA, a Ca^{2+}-

dx.doi.org/10.1021/bi201253b | Biochemistry 2011, 50, 9901−9910

specific scavenger, abolished the plasma membrane disintegrating activity of the NLPs.[22]

Having found a divalent cation in our crystal structure, although it has a different coordination pattern (Figure 2E), we set out to investigate what effect, if any, ions like zinc and calcium would have on the thermal stability and oligomeric state of MpMEP2 and if MpMEP2's necrotic activity is also dependent on calcium.

We first investigated the protein fold stability by determining its melting point using circular dichroism. Neither the presence of zinc nor the presence of calcium significantly altered the apparent melting temperature of MpNEP2 (T_{Mapp} for MpNEP2-$ZnCl_2$ = 41.2 °C, and T_{Mapp} for MpNEP2-$CaCl_2$ = 41.6 °C) relative to the thermal melting point measured in the absence of added divalent cations (T_{Mapp} for MpNEP2 = 39.9 °C) (Figure 3A). The thermal melting point was also obtained for MpNEP2 in the presence of EDTA to chelate any vestigial ions from the protein purification solutions (T_{Mapp} for MpNEP2-EDTA = 39.7 °C). The very similar apparent midpoints of the curves suggested that the presence of the tested cations did not affect the protein's conformational stability.

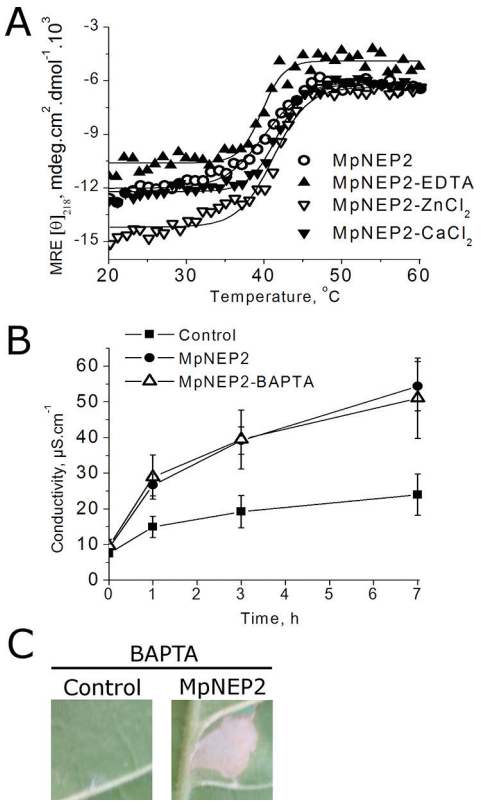

Figure 3. Structural stability, leakage, and necrosis promoting activity of ion-depleted MpNEP2 or MpNEP2 incubated with $CaCl_2$ or $ZnCl_2$. (A) Circular dichroism (CD) of MpNEP2, ion-depleted MpNEP2 (MpNEP2-EDTA), or MpNEP2 incubated with $CaCl_2$ or $ZnCl_2$ at λ = 218 nm measured over a range of temperatures. CD data (millidegrees) were converted to mean residue ellipticity units (MRE, millidegrees square centimeters per decimole) and plotted vs temperature. A sigmoidal curve was fitted, and the inflection point was calculated (T_{Mapp}), showing that ion binding does not influence protein stability and implying no structural role for the binding of the ion. (B) A vehicle solution with BAPTA, a specific Ca^{2+} chelator (Control), and vehicle solution with MpNEP2 (MpNEP2) or MpNEP2 and BAPTA (MpNEP2-BAPTA) was injected into tobacco leaves, and the electrolyte leakage was measured via solution conductivity. (C) A vehicle solution with BAPTA (Control) or a vehicle solution with MpNEP2 and BAPTA (MpNEP2) was injected into tobacco leaves, and the results were documented after 5 days. The data in panel B are the average values from three experiments ± SD, whereas the images in panel C are representative of three experiments.

Next, on the basis of the observations that zinc sits in a 2-fold symmetry center in our crystal structure and, consequently, that an MpNEP2 dimer can be generated by the crystal symmetry operations, we investigated what effects the ions mentioned above would have on the oligomeric state of the protein. Again, little to no change was observed in the hydrodynamic radii (R_H) measured for the protein either in the absence (2.2 nm, peak polydispersion of 4.4%) or in the presence of the cations ($CaCl_2$, 2.3 nm, peak polydispersion of 11%; $ZnCl_2$, 2.4 nm, peak polydispersion of 8.4%) and the chelating agent EDTA (2.3 nm, peak polydispersion of 10%). The calculated R_H value of the monomer, as determined by HYDROPRO using the monomer present in the asymmetric unit of our crystal, was 2.4 nm, leading us to conclude that, under the tested conditions, MpNEP2 is a monomer. The zinc-coordinated symmetric dimer in the crystal is therefore a packing artifact.

Finally, to check if the necrotic wound and electrolyte leakage promoting activities of MpNEP2 were dependent on calcium, the protein was injected into tobacco leaves both in the presence and in the absence of the calcium scavenger BAPTA. An electrolyte leakage assay was performed with leaves that were freshly treated with 10 mM BAPTA added to MpNEP2, and the results, when compared to the results of the same assay performed with MpNEP2 alone, indicated that this infiltration had no effect on the conductivity detected, as shown graphically in Figure 3B. These observations are supported by the images in Figure 3C, which show the detection of necrosis in leaves treated with MpNEP2 and 10 mM BAPTA but not when BAPTA was injected alone (control), clearly indicating that the addition of BAPTA to the vehicle solution did not perturb MpNEP2 activity.

Point Mutations Reveal Important Residues for MpNEP2 Activity. A comparison of the NLP primary sequences found in public databases revealed a strong conservation of a central heptapeptide motif, GHRHDWE,[14] which in MpNEP2 spans residues 115−121. Structurally, this peptide region comprises the bottom of the negatively charged cavity described in the previous section. The importance of this sequence for protein function has already been explored for NLP_{Pya}, for which the authors showed that substitution of either His101 or Asp104 (numbered according to its reference sequence) with alanine substantially abrogates its biological activity.[22] These His and Asp residues are two of the three residues that coordinate the divalent cation in Protein Data Bank entry 3gnz (Figure 2E), being His101 coordination via a water molecule. In the context of MpNEP2, only His116 (equivalent to His101 in NLP_{Pya}) coordinates the zinc ion.

We replaced His116 with either alanine (H116A) or serine (H116S) and Asp119 with a lysine (D119K), where both of these residues are from the conserved seven-residue sequence. The results revealed that all mutations of His116 and Asp119 in MpNEP2 disrupted the protein's ability to promote electrolyte leakage (Figure 4A) and necrotic wounds on tobacco leaves (Figure 4B). The mutation of the Asp119 residue to a lysine likely disturbed the negative potential of the cavity described above (Figure 2B), whereas changing the His116 to either a short nonpolar residue (alanine) or a negative polar residue

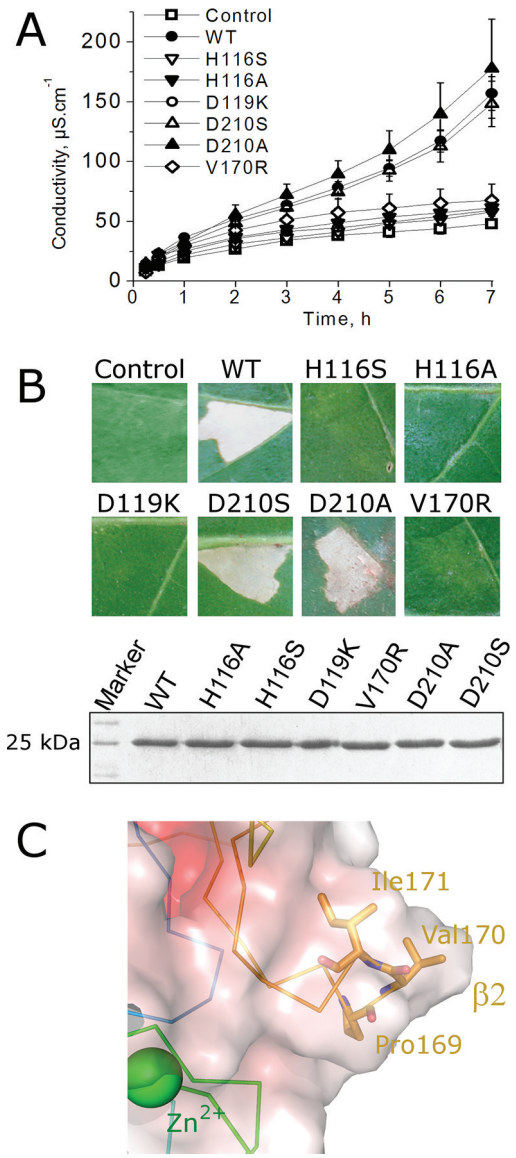

Figure 4. Mutation of residues from the acidic cavity and a hydrophobic loop disrupts MpNEP2 activity. (A) The vehicle solution (Control) or the vehicle solution containing wild-type (WT) MpNEP2 or mutant H116S, H116A, D119K, D210S, D210A, or V170R was injected into tobacco leaves, and the electrolyte leakage was measured by the solution conductivity for 7 h. (B) Additionally, the necrosis promoting activities on tobacco leaves were observed after 5 days. The bottom panel shows a Coomassie-stained SDS−PAGE gel that contained 50 μg of WT and mutant MpNEP2. The data in panel A are average values from three experiments ± SD, and the images in panel B are representative of three experiments. (C) Electrostatic potential surface representation of MpNEP2 β-hairpin β2 ($\pm 12 k_b T_C e^{-1}$), highlighting the hydrophobic β-turn composed of Pro169, Val170, and Ile171. The replacement of Val170 with an arginine residue disrupted protein activity.

(serine) has the potential to interfere with in vivo metal coordination, as found in our structure. To further test the importance of this coordination for protein activity, we replaced the other metal-coordinating residue, namely Asp210, with either alanine or serine. None of these mutations resulted in impaired protein activity (Figure 4A,B), implying that a cation is indeed dispensable for MpNEP2 activity, and H116 might exert its influence via a different mechanism. A circular dichroism analysis of melting temperatures of all mutant proteins assayed here revealed no notably altered tertiary structures within the mutant proteins, suggesting that the observed differences in the biological activities result from changes in the nearby vicinity of the altered residues (Figure S2 of the Supporting Information).

Finally, Kufner and co-workers hypothesized that the membrane attachment of NLP_{Pya} could be driven by a hydrophobic keel-like structure consisting of Trp155, Pro156, and Leu157 (according to their reference sequence), which would penetrate into the lipid core of the membrane like the hydrophobic regions of actinoporins and perfringolysin.[12] The equivalent residues in MpNEP2 are Pro169, Val170, and Ile171, respectively, which are structurally located at the turn of hairpin β2 (Figure 4C). To test this hypothesis, we replaced the apical residue in the turn, Val170, with an arginine. As shown in panels A and B of Figure 4, V170R MpNEP2 is impaired in its electrolyte leakage and necrosis promoting activities. To test MpNEP2's lipid binding capability, we performed EPR experiments with spin-labeled lipid vesicles and protein intrinsic fluorescence assays. The EPR spectra of the headgroup spin probe (DPPTC) or the acyl chain-labeled form (16-PC) incorporated into DOPC, DOPC/POPG (2:1 molar ratio), DOPC/POPS (2:1 molar ratio), or egg PC/DOPE (2:1 molar ratio) LUVs in the presence or absence of MpNEP2 showed no changes in their profile at a 1:100 protein:LUV molar ratio (Figure S3A of the Supporting Information). Similarly, the intrinsic fluorescence measurements of MpNEP2 indicated no significant perturbance in the tryptophan emission spectra after addition of a 100-fold molar excess of DOPC, DOPC/POPG, DOPC/POPS, or DOPC/DOPE unlabeled LUVs (Figure S3B of the Supporting Information).

DISCUSSION

Following the genome[10] and RNA sequencing analyses (Figure 1A) of *M. perniciosa*, five copies of NLPs were described, but only MpNEP2 was expressed during the cacao's Witches' Broom disease. A similar situation was described for *Phytophthora sojae* and *Phytophthora ramorum*, in which only a few of the more than 50 described genes are actually expressed during the diseases these organisms cause (stem and root rot of soybean and Sudden Oak Death, respectively).[14,39] The level of expression of MpNEP2 increases along with the necrotic symptoms, reaching its highest level during full necrosis just before the dry broom stage (Figure 1B). The transcripts encoding the necrosis-inducing protein of *P. sojae* (PsojNIP) reached their highest level after the transition of the fungus from the biotrophic to the necrotrophic stage in soybean plants,[40] whereas in *Mycosphaerella graminicola*, an NLP is expressed moments before necrosis symptoms occur.[41] The presence of more than one NEP-encoding gene in the studied genomes agrees with several evolutionary theories that have recently been grouped into a novel model, the "adaptive radiation model".[42] The other copies of the NEP-encoding gene are likely to be the result of recent duplications, having acquired different roles or become pseudogenes.

The founding member of the now-called NLP (NEP1-like protein) family was NEP1 (necrosis- and ethylene-inducing protein 1), which belongs to the organism *Fusarium oxysporum*.[43] The exact mode of action of NLPs during infection and virulence is not yet completely understood. The crystal structure of a NLP family member from the oomycete *Phytium aphanidermatum* (NLP_{Pya}) has recently been described,[22] and it

dx.doi.org/10.1021/bi201253b | *Biochemistry* 2011, 50, 9901−9910

was shown to resemble actinoporins, which are pore-forming toxins from marine invertebrates. The authors of this previous study concluded that NLPs are conserved virulence factors that cause plasma membrane permeabilization and cytolysis in plant cells with a mechanism that is dependent on the coordination of an ion, presumably calcium. As suggested, Ca^{2+} may mediate the docking of NLPs to target membranes, or it might, alternatively, be required for the membrane permeabilizing activity. Because plants seem to be capable of sensing the cellular changes induced by membrane damage, such as the release of host-derived endogenous elicitors or changes in ion homeostasis, NLPs probably trigger plant immunity-associated defenses through their interference with plant tissue integrity.[22] This idea would explain why so many authors had detected a defense response activity in hosts after they were challenged with NLPs.[13,14] The majority of genes that responded to NLPs are associated with general stress responses, which are calcium-dependent, and are actively expressed by plant host cells.[13,14]

Here, we described the crystal structure and mutational and functional studies of another member of the NLP family, MpNEP2, which is found in the causal agent of cacao's Witches' Broom disease, the fungus *M. perniciosa*. This disease is a serious concern to the South and Central American cacao crops, and an effective combat strategy has yet to be described. Like NLP_{Pya} and all the members of the NLP family, MpNEP2 has a conserved heptapeptide motif, GHRHDWE, which is shown to be part of a highly acidic groove (Figure 2B). In NLP_{Pya}, the residues from this motif coordinate an ion, likely Ca^{2+}, which was shown to be essential for protein activity. Although the crystal structure of MpNEP2 also included a cation in the vicinity of the acidic cavity, here we show that this protein does not depend on a cation for the promotion of its necrotic activity. The protein incubated with EDTA was as stable as the protein after the addition of either $ZnCl_2$ or $CaCl_2$ (Figure 3A), as measured by circular dichroism over a range of temperatures, indicating no structure-stabilizing function for these ions in MpNEP2. The wild-type calcium-depleted protein, as well as the Asp210A mutant in which one of the two ion-coordinating residues is replaced, behaved equally well in promoting tissue necrosis and electrolyte leakage when injected into tobacco leaves (Figures 3B,C and 4A,B). On the other hand, the mutation of the other ion-coordinating residue, His116, to either a serine or alanine did disrupt MpNEP2 activity, implying that His116 might be important for MpNEP2 necrotic activity via an alternative mechanism. The mutation of the Asp119 residue within the conserved heptapeptide to a nonpolar or oppositely charged residue disrupted protein activity (Figure 4A,B), reinforcing the importance of the negatively charged cavity for protein function.

The MpNEP2 structure is highly similar to the NLP_{Pya} structure (rsmd of 1.08 Å for Cα atoms). The latter[22] presented a fold highly conserved among the cytolytic actinoporins, especially the actinoporins produced by the sea anemones *Actinia equina* (equinatoxin II) and *Stichodactyla helianthus* (sticholysin II). Sticholysin II is a single-domain protein composed of a tightly folded core of β-sheet strands and two short α-helices, A and B, one on each side of the β-sandwich[44] (Figure S4A of the Supporting Information). The two-dimensional sticholysin II–lipid crystal data led to the proposal that the first 30 residues at the N-terminus, which encompass the amphiphilic α-helix A, are displaced from the body of the molecule upon binding of the lipid to be able to interact with the C-terminus of a neighboring molecule and form a tetramer.[44] The structural and functional data showed that the first contact of the molecule with the lipid membrane is promoted by the region around an exposed aromatic patch of the molecule, which contains tryptophan and tyrosine residues. The side chains of Trp110 and Trp114, which point downward and upward, respectively, with respect to the aromatic cluster, are exposed and very likely involved in the association of this protein region with lipid membranes[44] (Figure S4A of the Supporting Information) because the equivalent residues on equinatoxin II contribute to the fluorescence shifts observed upon lipid binding.[44,45] The crystal structure of sticholysin II complexed with phosphocholine revealed that the phospholipid headgroup binding site is placed exactly at this tryptophan and tyrosine rich segment[44] (Figure S4A of the Supporting Information).

In this work, we provide evidence that, remarkably, mutation of Val170 to an arginine residue abrogated protein necrosis and electrolyte activity, revealing that the triad consisting of Pro169, Val170, and Ile171 might, indeed, be a hydrophobic β-hairpin loop involved in membrane disruption. The aromatic patch described above for sticholysin II does not correlate structurally with the β-hairpin loop in MpNEP2 described here, which has a valine [Val170 (see Figure 4C)] that is important for protein activity (Figure 4A,B) (rmsd of 2.38 Å for Cα atoms upon superimposition of only the β-sheet core). Alternatively, this aromatic region fits within a region on MpNEP2 that has two tryptophan residues exposed to the solvent [Trp228 and Trp230 (Figure S4B of the Supporting Information)]. A possible scenario is that this segment of the protein, along with the hydrophobic β-hairpin loop [both are on the same side of the protein (see Figure S4B of the Supporting Information)], might be involved in the protein–lipid interaction. Moreover, to have a truly porin-like activity, in addition to being able to bind lipids, MpNEP2 must overcome its water-soluble conformation and transform into a lipophilic molecule. This transformation, induced by a lipid surface, would involve tertiary conformational changes. A deeper analysis of the MpNEP2 structural packing revealed that loop 2, as well as α-helix 2 and adjacent loops (Figure S4B of the Supporting Information), packs against the β-sheet core via aromatic stacking between several residues (Figure S4B of the Supporting Information, top right inset). A potential lipid-induced conformational change could displace this part of the protein to expose a lipophilic surface that was previously hidden.

However, EPR or intrinsic protein fluorescence studies conducted in the presence of LUVs containing phospholipids representative of the most common lipids found in plant cell membranes [32] showed no change in the spectra of the labeled lipids upon addition or MpNEP2 or protein tryptophan fluorescence after the incubation with the LUVs, respectively. Although we did not perform an exhaustive search of all types of lipids and their different combinations, these findings suggest that, if MpNEP2 anchors to the membrane to perform its necrotic activity, it likely requires an interaction with another membrane element, which could be either a specific membrane receptor or glycolipoprotein microdomains.[46,47] This finding could offer an explanation of how MpNEP2, as well as others NLPs, differentiates between dicotyledonous and monocotyledonous plants.[14]

During the progression of Witches' Broom disease, the fungal population inside the host becomes larger, and the concentration of molecules involved in quorum sensing signals also

increases. A phase change synchronization happens at this point of the disease, and MpNEP2 expression could be a benefit to *M. perniciosa* by releasing nutrients from lysed plant cells and by promoting an increase in the space that would allow the fungi's saprotrophic hyphae to quickly proliferate. The highly acidic cavity described for MpNEP2 and the hydrophobic Pro-Val-Ile loop are promising regions for compound screening and design because both of these regions have been shown to be essential for MpNEP2 necrosis promoting activity.

■ ASSOCIATED CONTENT

Supporting Information

Anomalous X-ray scattering data used to define the nature of the metals found in the structure (Figure S1), apparent melting temperatures measured by circular dichroism, as well as the CD profile at different wavelengths, of all of the mutants described in this paper (Figure S2), EPR and intrinsic fluorescence data in the presence and absence of LUVs (Figure S3), and structural comparisons between the actinoporin sticholysin II and MpNEP2 (Figure S4). This material is available free of charge via the Internet at http://pubs.acs.org.

Accession Codes

The atomic coordinates and diffraction data have been deposited in the Protein Data Bank as entry 3st1.

■ AUTHOR INFORMATION

Corresponding Author

*E-mail: sandra.dias@lnbio.org.br. Telephone: +55 19 3512 3503. Fax: +55 19 3512 1004.

Funding

This work was supported by FAPESP Grants 2010/51884-8 and 2009/50119-9 and Fellowships 2008/50995-0 and 2010/51891-4.

■ ACKNOWLEDGMENTS

We acknowledge the Spectroscopy and Calorimetry and the Robolab facilities at LNBio for technical assistance, as well as the staff of the D03B-MX1 beamline at the Brazilian National Synchrotron Laboratory. We give special thanks to Dr. Alessandra Girasole for the laboratory technical support.

■ ABBREVIATIONS

rmsd, root-mean-square deviation; NLPs, NEP1-like proteins; DAI, days after inoculation of *T. cacao* with *M. perniciosa* spores; SD, standard deviation; WBD, Witches' Broom disease.

■ REFERENCES

(1) Griffith, G. W., Nicholson, J., Nenninger, A., Birch, R. N., and Hedger, J. N. (2003) Witches' brooms and frosty pods: Two major pathogens of cacao. *N. Z. J. Bot. 41* (3), 423−435.

(2) Pereira, J. L., Ram, A., Figuereido, J. M., and de Almeida, L. C. (1989) La primera aparición de la "escoba de bruja" en la principal área productora de cacao del Brasil. *Turrialba 39* (7), 459−461.

(3) Meinhardt, L. W., Rincones, J., Bailey, B. A., Aime, M. C., Griffith, G. W., Zhang, D., and Pereira, G. A. G. (2008) *Moniliophthora perniciosa*, the causal agent of witches' broom disease of cacao: What's new from this old foe? *Mol. Plant Pathol. 9* (5), 577−588.

(4) Aime, M. C., and Phillips-Mora, W. (2005) The causal agents of witches' broom and frosty pod rot of cacao (chocolate, *Theobroma cacao*) form a new lineage of Marasmiaceae. *Mycologia 97* (5), 1012−1022.

(5) Purdy, L. H., and Schmidt, R. A. (1996) Status of cacao witches' broom: Biology, epidemiology, and management. *Annu. Rev. Phytopathol. 34*, 573−594.

(6) Scarpari, L. M., Meinhardt, L. W., Mazzafera, P., Pomella, A. W., Schiavinato, M. A., Cascardo, J. C., and Pereira, G. A. (2005) Biochemical changes during the development of witches' broom: The most important disease of cocoa in Brazil caused by *Crinipellis perniciosa*. *J. Exp. Bot. 56* (413), 865−877.

(7) Delgado, J. C., and Cook, A. A. (1976) Nuclear condition of basidia, basidiospores, and mycelium of *Marasmius perniciosus*. *Can. J. Bot. 54* (1−2), 66−72.

(8) Evans, H. C. (1980) Pleomorphism in *Crinipellis perniciosa*, Causal Agent of Witches Broom Disease of Cocoa. *Trans. Br. Mycol. Soc. 74* (6), 515−523.

(9) Griffith, G. W., and Hedger, J. N. (1994) Dual culture of *Crinipellis perniciosa* and potato callus. *Eur. J. Plant Pathol. 100* (6), 371−379.

(10) Mondego, J. M., Carazzolle, M. F., Costa, G. G., Formighieri, E. F., Parizzi, L. P., Rincones, J., Cotomacci, C., Carraro, D. M., Cunha, A. F., Carrer, H., Vidal, R. O., Estrela, R. C., Garcia, O., Thomazella, D. P., de Oliveira, B. V., Pires, A. B., Rio, M. C., Araujo, M. R., de Moraes, M. H., Castro, L. A., Gramacho, K. P., Gonçalves, M. S., Neto, J. P., Neto, A. G., Barbosa, L. V., Guiltinan, M. J., Bailey, B. A., Meinhardt, L. W., Cascardo, J. C., and Pereira, G. A. (2008) A genome survey of *Moniliophthora perniciosa* gives new insights into witches' broom disease of cacao. *BMC Genomics 9*, 548.

(11) Garcia, O., Macedo, J. A., Tiburcio, R., Zaparoli, G., Rincones, J., Bittencourt, L. M., Ceita, G. O., Micheli, F., Gesteira, A., Mariano, A. C., Schiavinato, M. A., Medrano, F. J., Meinhardt, L. W., Pereira, G. A., and Cascardo, J. C. (2007) Characterization of necrosis and ethylene-inducing proteins (NEP) in the basidiomycete *Moniliophthora perniciosa*, the causal agent of witches' broom in *Theobroma cacao*. *Mycol. Res. 111* (4), 443−455.

(12) Kufner, I., Ottmann, C., Oecking, C., and Nurnberger, T. (2009) Cytolytic toxins as triggers of plant immune response. *Plant Signaling Behav. 4* (10), 977−979.

(13) Pemberton, C. L., and Salmond, G. P. (2004) The Nep1-like proteins: A growing family of microbial elicitors of plant necrosis. *Mol. Plant Pathol. 5*, 353−359.

(14) Gijzen, M., and Nurnberger, T. (2006) Nep1-like proteins from plant pathogens: Recruitment and diversification of the NPP1 domain across taxa. *Phytochemistry 67*, 1800−1807.

(15) Frias, G. A., Purdy, L. H., and Schmidt, R. A. (1995) An inoculation method for evaluating resistance of cacao to *Crinipellis perniciosa*. *Plant Dis. 79* (8), 787−791.

(16) Azevedo, H., Lino-Neto, T., and Tavares, R. M. (2003) An improved method for high-quality RNA isolation from needles of adult maritime pine trees. *Plant Mol. Biol. Rep. 21*, 333−338.

(17) Livac, K. J., and Schmittgen, T. D. (2001) Analysis of relative gene expression data using real-time quantitative PCR and the 2^{2DDCT} method. *Methods 25*, 402−408.

(18) Gasteiger, E., Hoogland, C., Gattiker, A., Duvaud, S., Wilkins, M. R., Appel, R. D., and Bairoch, A. (2005) Protein Identification and Analysis Tools on the ExPASy Server. In *The Proteomics Protocols Handbook* (Walker, J. M., Ed.) pp 571−607, Humana Press, Totowa, NJ.

(19) Leslie, A. G. W. (1992) Recent changes to the MOSFLM package for processing film and image plate data, *Joint CCP4 + ESF-EAMCB Newsletter on Protein Crystallography*, Vol. *26*.

(20) Evans, P. R. (2005) Scaling and assessment of data quality. *Acta Crystallogr. D62*, 72−82.

(21) McCoy, A. J., Grosse-Kunstleve, R. W., Adams, P. D., Winn, M. D., Storoni, L. C., and Read, R. J. (2007) Phaser crystallographic software. *J. Appl. Crystallogr. 40*, 658−674.

(22) Ottmann, C., Luberacki, B., Kufner, I., Koch, W., Brunner, F., and Weyand, M. (2009) A common toxin fold mediates microbial attack and plant defense. *Proc. Natl. Acad. Sci. U.S.A. 106*, 10359−10364.

(23) Zhang, K. Y. J., Cowtan, K., and Main, P. (1997) Combining constraints for electron-density modification. *Methods Enzymol. 277*, 53−64.
(24) Collaborative Computational Project, Number 4 (1994) The CCP4 Suite: Programs for Protein Crystallography. *Acta Crystallogr. D50*, 760−763.
(25) Perrakis, A., Morris, R. M., and Lamzin, V. S. (1999) Automated protein model building combined with iterative structure refinement. *Nat. Struct. Biol. 6*, 458−463.
(26) Vagin, A. A., Steiner, R. S., Lebedev, A. A., Potterton, L., McNicholas, S., Long, F., and Murshudov, G. N. (2004) REFMAC5 dictionary: Organisation of prior chemical knowledge and guidelines for its use. *Acta Crystallogr. D60*, 2284−2295.
(27) Emsley, P., Lohkamp, B., Scott, W. G., and Cowtan, K. (2010) Features and development of Coot. *Acta Crystallogr. D66*, 486−501.
(28) Read, R. J., and Schierbeek, A. J. (1988) *J. Appl. Crystallogr. 21*, 490−495.
(29) Chen, V. B., Arendall, W. B. III, Headd, J. J., Keedy, D. A., Immormino, R. M., Kapral, G. J., Murray, L. W., Richardson, J. S., and Richardson, D. C. (2010) MolProbity: All-atom structure validation for macromolecular crystallography. *Acta Crystallogr. D66*, 12−21.
(30) Whitmore, L., and Wallace, B. A. (2008) Protein Secondary Structure Analyses from Circular Dichroism Spectroscopy: Methods and Reference Databases. *Biopolymers 89*, 392−400.
(31) Ortega, A., Amoros, D., and Garc1a de la Torre, J. (2011) Prediction of hydrodynamic and other solution properties of rigid proteins from atomic- and residue-level models. *Biophys. J. 101*, 892−898.
(32) Welti, R., Li, W., Li, M., Sang, Y., Biesiada, H., Zhou, H. E., Rajashekar, C. B., Williams, T. D., and Wang, X. (2002) Profiling membrane lipids in plant stress responses. Role of phospholipase Dα in freezing-induced lipid changes in *Arabidopsis*. *J. Biol. Chem. 277* (35), 31994.
(33) Simon, E. W. (1974) Phospholipids and plant membrane permeability. *New Phytol. 73*, 377.
(34) Marchler-Bauer, A., Lu, S., Anderson, J. B., Chitsaz, F., Derbyshire, M. K., Deweese-Scott, C., Fong, J. H., Geer, L. Y., Geer, R. C., Gonzales, N. R., Gwadz, M., Hurwitz, D. I., Jackson, J. D., Ke, Z., Lanczycki, C. J., Lu, F., Marchler, G. H., Mullokandov, M., Omelchenko, M. V., Robertson, C. L., Song, J. S., Thanki, N., Yamashita, R. A., Zhang, D., Zhang, N., Zheng, C., and Bryant, S. H. (2011) CDD: A Conserved Domain Database for the functional annotation of proteins. *Nucleic Acids Res. 39*, D225−D229.
(35) Baker, N. A., Sept, D., Joseph, S., Holst, M. J., and McCammon, J. A. (2001) Electrostatics of nanosystems: Application to microtubules and the ribosome. *Proc. Natl. Acad. Sci. U.S.A. 98*, 10037−10041.
(36) Voss, N. R., and Gerstein, M. (2010) 3V: Cavity, channel and cleft volume calculator and extractor. *Nucleic Acids Res. 38*, W555−W562.
(37) Krissinel, E., and Henrick, K. (2007) Inference of macromolecular assemblies from crystalline state. *J. Mol. Biol. 372*, 774−797.
(38) Kabsch, W. (1976) A solution for the best rotation to relate two sets of vectors. *Acta Crystallogr. A32*, 922−923.
(39) Bae, H., Bowers, J. H., Tooley, P. W., and Bailey, B. A. (2005) NEP1 orthologs encoding necrosis and ethylene inducing proteins exist as a multigene family in *Phytophthora megakarya*, causal agent of black pod disease on cacao. *Mycol. Res. 109*, 1373−1385.
(40) Qutob, D., Kamoun, S., and Gijzen, M. (2002) Expression of a *Phytophthora sojae* necrosis-inducing protein occurs during transition from biotrophy to necrotrophy. *Plant J. 32*, 361−373.
(41) Motteram, J., Kufner, I., Deller, S., Brunner, F., Hammond-Kosack, K. E., and Nürnberger, T. (2009) Molecular characterization and functional analysis of MgNLP, the sole NPP1 domain-containing protein, from the fungal wheat leaf pathogen *Mycosphaerella graminicola*. *Mol. Plant-Microbe Interact. 22*, 790−799.
(42) Francino, M. P. (2005) An adaptive radiation model for the origin of new gene functions. *Nat. Genet. 37*, 573−578.
(43) Bailey, B. (1995) Purification of a protein from culture filtrates of *Fusarium oxysporum* that induces ethylene and necrosis in leaves of *Erythroxylum coca*. *Phytopathology 85*, 1250−1255.
(44) Mancheño, J. M., Martín-Benito, J., Martínez-Ripoll, M., Gavilanes, J. G., and Hermoso, J. A. (2003) Crystal and Electron Microscopy Structures of Sticholysin II Actinoporin Reveal Insights into the Mechanism of Membrane Pore Formation. *Structure 11*, 1319−1328.
(45) Malovrh, P., Barlic, A., Podlesek, Z., Macek, P., Menestrina, G., and Anderluh, G. (2000) Structure−function studies of tryptophan mutants of equinatoxin II, a sea anemone pore-forming protein. *Biochem. J. 346*, 223−232.
(46) Mongrand, S., Morel, J., Laroche, J., Claverol, S., Carde, J. P., Hartmann, M. A., Bonneu, M., Simon-Plas, F., Lessire, R., and Bessoule, J. J. (2004) Lipid rafts in higher plant cells: Purification and characterization of Triton X-100-insoluble microdomains from tobacco plasma membrane. *J. Biol. Chem. 279* (35), 36277.
(47) Bhat, R. A., and Panstruga, R. (2005) Lipid rafts in plants. *Planta 223*, 5.